AGU ADVANCING EARTH AND SPACE SCIENCE

Geophysical Research Letters®

RESEARCH LETTER
10.1029/2021GL096977

**Key Points:**

- Magnetic enhancement of alluvial sediments in the Teruel Basin is likely caused by formation of ferrimagnetic minerals during pedogenesis
- First high resolution late Pliocene terrestrial environmental magnetism paleoclimatic record from southwestern Europe
- Contrasting dominant orbital cycles in Spain between early and late Pliocene

**Supporting Information:**

Supporting Information may be found in the online version of this article.

**Correspondence to:**

J. Nie,
jnie@lzu.edu.cn

**Citation:**

Gao, P., Nie, J., Breecker, D. O., Gallagher, T., Serach, L., & Alonso-Zarza, A. M. (2022). Similar magnetic enhancement mechanisms between Chinese loess and alluvial sediments from the Teruel Basin, NE Spain, and paleoclimate implications. *Geophysical Research Letters*, *49*, e2021GL096977. https://doi.org/10.1029/2021GL096977

Received 9 NOV 2021
Accepted 8 MAR 2022

**Author Contributions:**

**Funding acquisition:** Junsheng Nie, Daniel O. Breecker
**Investigation:** Peng Gao, Junsheng Nie, Daniel O. Breecker, Timothy Gallagher, Lily Serach, Ana M. Alonso-Zarza
**Project Administration:** Junsheng Nie, Daniel O. Breecker
**Writing – original draft:** Peng Gao, Junsheng Nie
**Writing – review & editing:** Peng Gao, Junsheng Nie, Daniel O. Breecker, Timothy Gallagher, Ana M. Alonso-Zarza



# Similar Magnetic Enhancement Mechanisms Between Chinese Loess and Alluvial Sediments From the Teruel Basin, NE Spain, and Paleoclimate Implications

**Peng Gao[1], Junsheng Nie[1], Daniel O. Breecker[2], Timothy Gallagher[2,3], Lily Serach[2], and Ana M. Alonso-Zarza[4]**

[1]Key Laboratory of Western China's Environment System (Ministry of Education), College of Earth and Environmental Sciences, Lanzhou University, Lanzhou, China, [2]Department of Geological Sciences, University of Texas at Austin, Austin, TX, USA, [3]Department of Geology, Kent State University, Kent, OH, USA, [4]Instituto Geológico y Minero de España, IGME, Madrid, Spain

**Abstract** The Pliocene is considered an analog for future climate. Insolation is found the dominant forcing for Asian precipitation over the late Pliocene, evidenced by magnetic enhancement of Chinese loess caused by formation of nanometer-scale ferrimagnetic grains during pedogenesis corresponding to high precipitation. However, lack of European loess limits understanding of Pliocene European climate. We identified likely similar magnetic enhancement mechanism between Pliocene alluvial sediments from Spain and Chinese loess despite different depositional settings. This provides an opportunity to improve understanding of Pliocene climate in Europe. Spectral analysis shows that European wet-dry variations during the early Pliocene were forced by insolation and during the late Pliocene by both insolation and ice sheets development. During the Quaternary, in contrast, the forcing was dominantly from high latitude. These results demonstrate the importance of insolation during warm climates and the growing importance of ice sheets with global cooling in controlling Northern Hemisphere precipitation changes.

**Plain Language Summary** Loess plays an important role in understanding past environmental variations in China. However, loess records in Europe extending back to the warm Pliocene, a potential analog interval to future climate, are lacking. Here we find that the magnetic susceptibility enhancement mechanism for a set of distal alluvial fan sediments in the Teruel Basin of northeastern Spain is similar to that of Chinese loess. This provides us a unique chance to understand environmental variation during the Pliocene in Europe. We found that insolation plays a more important role than high latitude ice sheets over the Pliocene in comparison with the Quaternary. Together with paleoenvironmental records from the other parts of Europe and China, these results reveal that Northern Hemisphere (NH) environment variations over the Pliocene were consistently controlled mainly by insolation. This finding has implications for understanding how the future environment in the NH will react to high and low latitude forcing.

## 1. Introduction

The Pliocene is considered a potential analog for future climate and the Pliocene Model Intercomparison Project (PlioMIP) working group has formed specifically focused on understanding climate of this interval (Dowsett et al., 1994, 2010, 2016; Haywood et al., 2010, 2016). Generating high resolution paleoclimate records over the Pliocene period is an important task of the paleoclimate community.

Magnetic parameter records have played a key role in extracting Pliocene East Asian monsoon variations from Chinese loess sequences (An et al., 2001; Guo et al., 2002; Sun et al., 2006). Many recent studies demonstrate that magnetic enhancement of the Pliocene loess (also called red clay due to its reddish color) is caused by neoformation of nanometer-scale ferromagnetic grains (magnetite and maghemite) during pedogenic process (Nie et al., 2007), similar to the overlying loess-paleosol sequences deposited over the Quaternary (Bloemendal & Liu, 2005; Liu et al., 2004; Maher & Taylor, 1988). Particularly, the content of nanometer-scale ferromagnetic grains is strongly correlated with annual mean precipitation, whereas its correlation with annual mean temperature is weak (Nie et al., 2010). Therefore, magnetic susceptibility records are proposed to be able to record precipitation variations on the Chinese Loess Plateau (CLP), which are caused by intensity variations of the East Asian summer monsoonal circulation (An et al., 2001; Bloemendal & Liu, 2005; Maher & Taylor, 1988;

Sun et al., 2006). However, the Pliocene is characterized by higher air temperature and smaller amplitude of temperature variations than the Quaternary, resulting in more magnetic minerals transforming to hematite. As a result, magnetic susceptibility, which shows apparent orbital timescale variations in the Quaternary loess-paleosol sequences on the CLP, shows weak orbital timescale variations for the Pliocene red clay sequences (Sun et al., 2006). In order to extract orbital band precipitation variations from the Pliocene red clay sequences, Luo et al. (2020) used content ratio of ultrafine ferromagnetic minerals over hematite (represented by $\chi_{fd}$/HIRM) as a precipitation proxy and reconstructed precipitation variations over the middle Piacenzian. The records show prominent precessional band cycles. This benefits from the introduction of the $\chi_{fd}$/HIRM proxy which represents the content variation of magnetic minerals produced by wetter climate over those produced by drier climate (Liu et al., 2013; Nie et al., 2017, 2020).

European sites do not have continuous loess records over the Pliocene (Li et al., 2020) and understanding of past environmental variations focused mostly on the lacustrine sediments over the Quaternary (Palchan et al., 2017; Waldmann et al., 2009). Few records are available for the Pliocene interval, with some exception of discontinuous or low resolution pollen records (Jiménez-Moreno et al., 2010, 2013, 2019; Salzmann et al., 2011; Suc, 1984; Suc & Popescu, 2005), preventing a full understanding of the Pliocene precipitation variations in European region. Although many workers used Mediterranean records to infer past environmental variations, these records are mostly affected by African monsoons (Colleoni et al., 2012; Emeis et al., 2000; Herbert et al., 2015; Rossignolstrick, 1983, 1985). Therefore, high resolution records recording orbital-band paleoclimate variations in other European region are rare. Finding the right proxy to reconstruct paleo-precipitation or finding new archives would deepen our understanding of past environmental changes in this region. Here we target magnetic property analysis of a set of alluvial sediments over the Pliocene in the Teruel Basin in order to promote understanding of past environments in this area.

One surprising finding is that the magnetic enhancement mechanisms of the alluvial sediments in the Villalba Alta (VA) section of the Teruel Basin (Figure S1 in Supporting Information S1) is similar to the Chinese loess sediments on the CLP. This gives us an opportunity to explore the underlying environmental variation signal from this set of sediments and compare underlying forcing mechanisms across both European and Asian sites.

## 2. Geographic and Geologic Setting

The Teruel Basin, which is located on the eastern Iberian Peninsula (northeastern Spain; Figure S1a in Supporting Information S1), covers an area of about 100 km in length and 15 km in width (Figure S1b in Supporting Information S1; Alonso-Zarza & Calvo, 2000; Alonso-Zarza et al., 2012; Van Dam et al., 2001). The formation of the basin is related to the extensional tectonics linked to the rifting of the Valencia Trough (western Mediterranean Sea) during the Miocene (Anadón et al., 1989; Roca & Guimerà, 1992). There are many active normal faults trending NNE-SSW and NNW-SSE located in the eastern parts of the basin, and the basin is regarded as an intra-mountain graben trending NNE-SSW (Ezquerro et al., 2014, 2019). The basin is filled by a Neogene succession with a thickness of 500 m, consisting of siliciclastic, carbonate, and gypsum deposits from alluvial fan and shallow lacustrine environment (Ezquerro et al., 2014, 2019). The Teruel Basin region currently belongs to the middle mountainous Mediterranean climatic domain (Domingo et al., 2009), which is characterized by wet winters and dry summers.

The studied VA section is located at the northern margin of the Teruel Basin (Figure S1b in Supporting Information S1). The bottom of the section is located at 40º 36'54"N, 0° 58'33"W, which is to the south of the road that crosses the escarpment west of VA and the top of the section is located by the hairpin turn in the road just above the escarpment (Figure S2 in Supporting Information S1). Previous paleomagnetic work has assigned a late Pliocene to early Pleistocene depositional age range for this set of strata (Opdyke et al., 1997). We found a more continuous section about 520 m south of the outcrop studied by Opdyke et al. (1997), which constitutes the research focus of our study (Figure S2 in Supporting Information S1).

## 3. Materials and Methods

The VA section consists of two depositional environments: alluvial fan (Unit II 13.2–22.4 m and Unit IV 35.4–90.6 m) and lacustrine (Unit I 0–13.2 m and Unit III 22.4–35.4 m; Figure 1). Unit I consists of gray soft limestone and hard white limestones, interpreted as shallow lacustrine environment. Unit II consists of red mudstone and

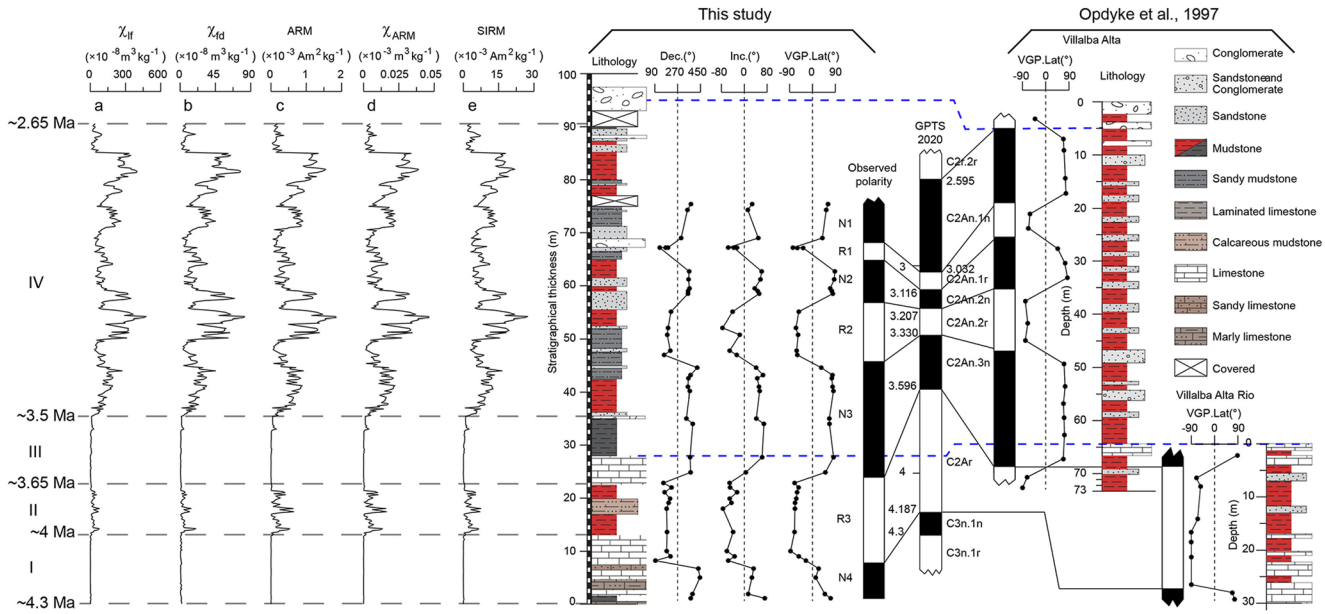


**Figure 1.** Magnetic parameters, lithology, and age model from the Villalba Alta (VA) section. The left panel shows the magnetic parameters. (a) $\chi_{lf}$, (b) $\chi_{fd}$, (c) anhysteretic remanent magnetization (ARM), (d) $\chi_{ARM}$, (e) saturation isothermal remanent magnetization. The right panel shows lithology and magnetostratigraphic results for the VA section. VGP: virtual geomagnetic polarity; GPTS: geomagnetic polarity time scale (Ogg, 2020). Blue dashed lines represent two maker layers (limestone and conglomerate).

calcareous mudstone, interpreted as alluvial environment. Unit III consists of laminated limestone at the bottom half and black mudstone at the top half, typical sediments of lacustrine setting. Unit IV consists of red mudstone, sandy mudstone, sandstone, and some conglomerates. Carbonate nodules and root traces are commonly observed in this unit. We interpret this unit as alluvial setting, consistent with previous interpretation (Alonso-Zarza & Arenas, 2004; Ezquerro et al., 2019).

Environmental magnetism samples were obtained at an interval of 20 cm from the VA section with thickness of 90.6 m. In the laboratory, the samples were crushed and packed in the non-magnetic boxes of 2 × 2 × 2 cm for magnetic measurements. We measured the low and high frequency magnetic susceptibility ($\chi_{lf}$ and $\chi_{hf}$), saturation isothermal remanent magnetization (SIRM) and anhysteretic remanent magnetization (ARM) of these samples (see Text S1 in Supporting Information S1). Frequency-dependent magnetic susceptibility ($\chi_{fd}$) can be calculated as $\chi_{fd} = \chi_{lf} - \chi_{hf}$, which can indicate content of nanometer-scale ferrimagnets close to superparamagnetic and stable single domain boundary (Bloemendal et al., 1992). The ARM is often expressed as the ARM susceptibility ($\chi_{ARM}$), which is obtained by normalizing to the 0.05 mT direct bias field. The $\chi_{ARM}$ values are sensitive to the stable single domain (SD) and smaller pseudo single domain (PSD) ferrimagnetic mineral concentration (such as magneite or maghemite). Detailed rock magnetic experiments, including stepwise isothermal remanent magnetization (IRM) acquisition curves, hysteresis loops, and first-order reversal curve (FORC) diagrams, were performed on the representative samples at different stratigraphical levels and lithology to identify the magnetic minerals of sediments in the VA section (see Text S2 in Supporting Information S1).

Paleomagnetic samples were taken at 1–3 m intervals from the VA section using a portable battery-powered drill and were oriented with a Brunton compass in the field. We note that no paleomagnetic sample was obtained for the 75.4–90.6 m formation because rocks are too fragile. For the limestone-dominated intervals, we focused on sampling gray-colored limestone and avoided the white limestone with the assumption that magnetic minerals are partially preserved in gray-colored limestone but have been completely dissolved for white limestone intervals. The oriented samples were subjected to systematic stepwise thermal demagnetization (see Text S3 in Supporting Information S1).

To identify dominant frequencies, we performed spectral analysis on the $\chi_{fd}$ time series of the VA section with software Acycle v2.2 (Li et al., 2019). The detailed steps are shown in Text S4 in Supporting Information S1.

# 4. Results

## 4.1. Age Model

The age model has been established by Opdyke et al. (1997), and there are two marker layers (Figure S2 in Supporting Information S1) that allow us to correlate our section to the one studied by Opdyke et al. (1997). Therefore, the age model of our section has been pre-determined by the work by Opdyke et al. (1997). The demagnetization results of representative specimens are shown in Figure S3 in Supporting Information S1. Positive bootstrap reversal test (Tauxe, 1998) results indicate that we recovered the primary characteristic remanent magnetizations (ChRMs; Figure S4 in Supporting Information S1). Four normal and three reversed polarities are observed from the VA section (Figure 1), and these polarity intervals can be readily correlated to the established age model by Opdyke et al. (1997). We further update the age model using the geomagnetic polarity time scale 2020 (GPTS 2020; Ogg, 2020). According to this correlation pattern, the four normal polarities N1, N2, N3, and N4 should correspond to C2An.1n, C2An.2n, C2An.3n, and C3n.1n of the GPTS 2020 (Figure 1), respectively. The reversed polarities R1, R2, and R3 can then correspond to C2An.1r, C2An.2r, and C2Ar (Figure 1), respectively. The limitations of the paleomagnetic data and the age model is discussed in Text S5 in Supporting Information S1.

The ages of the strata with a thickness of 90.6 m span from 4.3 Ma to 2.65 Ma (Figure 1 and Figures S5 in Supporting Information S1). We note that the ages for strata of 0–7.85 m and 69–90.6 m were based on extrapolation and thus have large uncertainties (Text S5 in Supporting Information S1). However, the interval 7.85–69 m are bracketed by the reversal ages, which correspond to the time interval 4.187–3.032 Ma. Thus, spectral analysis was performed only on the interval 4.187–3.032 Ma.

## 4.2. Environmental Magnetism Records

Figure 1 and Figure S5 in Supporting Information S1 show the variations of the magnetic parameters from the VA section, which can be divided into four intervals (Figure 1): 4.3–4 Ma (Unit I, 0–13.2 m), 4–3.65 Ma (Unit II, 13.2–22.4 m), 3.65–3.5 Ma (Unit III, 22.4–35.4 m), and 3.5–2.65 Ma (Unit IV, 35.4–90.6 m). These intervals are consistent with lithology divisions (Figure 1). In Units I and III, magnetic parameter values are close to zero. Magnetic parameter values increase in Unit II, but lower than those in Unit IV. $\chi_{lf}$, $\chi_{fd}$, ARM, $\chi_{ARM}$ and SIRM exhibit strong linear correlation in alluvial fan sediments (Units II and IV; Figures 2a–2d), but they exhibit weak correlation in lacustrine sediments (Units I and III; Figures 2e–2h).

IRM acquisition curves, hysteresis loops, and FORC diagrams provide insights into the magnetic mineralogy for the alluvial and lacustrine units. For alluvial samples, the magnetic minerals are dominated by superparamagnetic (SP) and stable single-domain (SSD) ferrimagnetic particles (Figure S6 in Supporting Information S1). For lacustrine sediments, however, the concentration of ferrimagnetic minerals is low, and the content of hematite is higher (Figure S6 in Supporting Information S1). The detailed explanations for the rock magnetic experiments are shown in Text S2 in Supporting Information S1.

## 4.3. Spectral Analysis

We performed spectral analysis on the $\chi_{fd}$ record, a proxy that we will use for precipitation variations in this region, as we will explain later, for the intervals 4–3.65 (early Pliocene) and 3.5–3.05 Ma (late Pliocene), which have good age control. Our average sampling resolution is ~7.4 ka for the interval from 4 to 3.65 Ma and ~3.2 ka for the interval of 3.5–3.05 Ma. However, we observe clear precessional cycles over the low resolution interval 4–3.65 Ma. Furthermore, the interval 4–3.65 Ma is characterized by strong 100-kyr-band but weak 41-kyr cycles (Figure 3 and Figure S7a in Supporting Information S1). Two non-Milankovitch signals (63 and 29 kyr) also exist likely because of harmonics of main orbital cycles (Figure S7a in Supporting Information S1). By contrast, we observe weak precessional cycles over the high-resolution interval 3.5–3.05 Ma (Figure 3 and Figure S7b in Supporting Information S1); particularly, the interval 3.3–3.18 Ma (highlighted by three vertical gray bars) is characterized by strong 41-kyr cycles but weak 20- and 100-kyr-band cycles (Figure 3 and Figure S7b in Supporting Information S1).

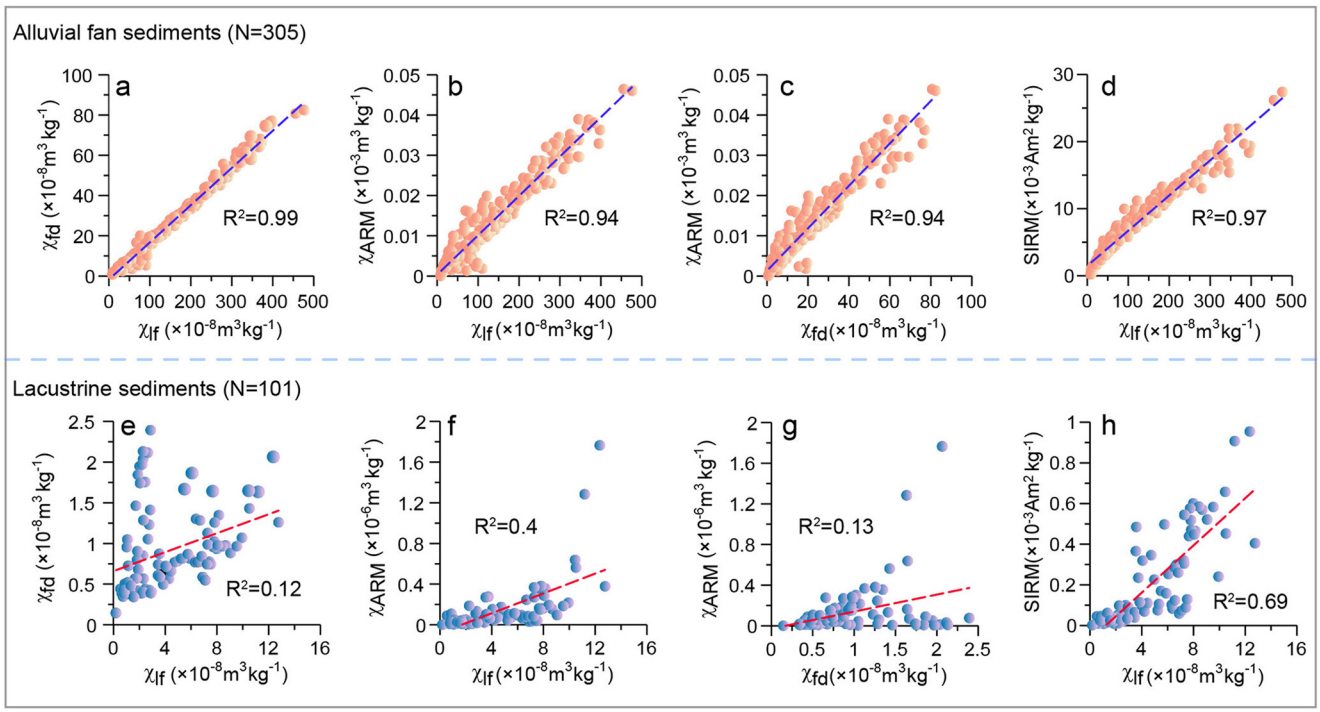


**Figure 2.** The relationship between $\chi_{lf}$ versus $\chi_{fd}$, $\chi_{lf}$ versus $\chi_{ARM}$, $\chi_{fd}$ versus $\chi_{ARM}$ and $\chi_{lf}$ versus saturation isothermal remanent magnetization in the Villalba Alta section. (a–d) alluvial fan sediments (II and IV); (e–h) lacustrine sediments (I and III). N: Number of samples.

## 5. Discussion

### 5.1. Magnetic Enhancement Mechanisms of the Alluvial Sediments of the VA Section

One surprising finding is that $\chi_{lf}$ shows strong correlation with $\chi_{fd}$ and $\chi_{ARM}$ in the VA section (Figure 2), similar to the pattern on the CLP (Liu et al., 2004; Nie et al., 2007), despite that the VA site is far from the CLP and the climates of these two locations are not similar.

It is well known that magnetic enhancement in the sediments on the CLP was caused by production of nanometer-scale ferrimagnetic particles during pedogenesis (Liu et al., 2004; Nie et al., 2007). Magnetic susceptibility increase in Chinese loess is attributed to monsoonal climate (Ahmed & Maher, 2018; Zhou et al., 1990), which can produce many oxidation-reduction cycles associated with seasonal precipitation followed by climate drying. Some propose a different magnetic enhancement mechanism for Chinese loess: ferrihydrite converted to → maghemite (Barrón et al., 2003; Hu et al., 2013; Torrent et al., 2006). However, recent electron microscope evidence demonstrates limited maghemite grains in the nanometer-scale grains of Chinese loess (Ahmed & Maher, 2018); instead, the nanometer-scale ferrimagnetic grains in Chinese loess are magnetite. Therefore, this new evidence is consistent with linking magnetic susceptibility enhancement of Chinese loess to monsoonal precipitation which produces many oxidation-reduction cycles (Maher, 1998; Maher & Taylor, 1988).

The similar correlation pattern between magnetic parameters (strong correlation between $\chi_{lf}$ and $\chi_{fd}$, $\chi_{lf}$ and $\chi_{ARM}$, $\chi_{fd}$ and $\chi_{ARM}$, $\chi_{lf}$ and SIRM) in the Spain section suggests a similar magnetic enhancement mechanism as the CLP. We argue that seasonal dry and wet variation can also produce the oxidation-reduction cycles responsible for production of nanometer-scale ferrimagnetic grains in the Teruel Basin. In winters, when abundant precipitation fills pore space of the alluvial fan sediments, a reducing environment forms and $Fe^{3+}$ can be reduced to $Fe^{2+}$. Then, in summers, dry climate creates oxidic environment in pore spaces of the alluvial fan sediments. Therefore, nanometer-scale magnetite can form in this situation and the amount of nanometer-scale magnetite is controlled by how many $Fe^{2+}$ ions can form (because $Fe^{3+}$ is readily available in soils receiving seasonal precipitation). This explains the link between high magnetic susceptibility and precipitation amount, both for Chinese loess and for the alluvial fan sediments in Spain. The existence of many layers of pedogenic carbonate including cemented carbonate, calcite nodules, clast coatings and filaments in this section (Alonso-Zarza & Arenas, 2004),

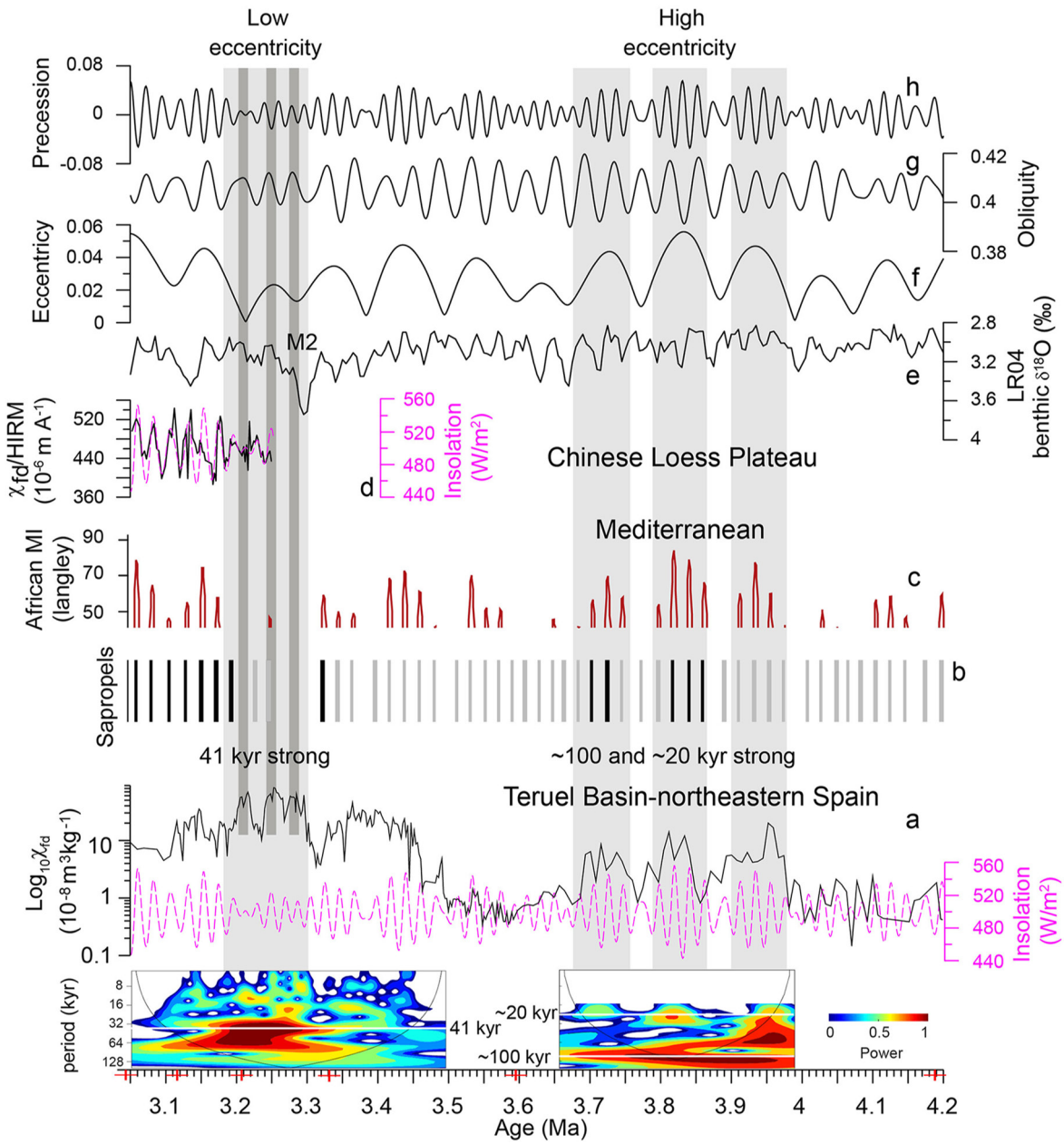


**Figure 3.** Comparison of the paleoclimate records from (a) Teruel Basin (this study); (b–c) Mediterranean (Colleoni et al., 2012; Emeis et al., 2000; Rossignol-Strick, 1983, 1985); (d) Chinese Loess Plateau (Luo et al., 2020); (e) Marine benthonic $\delta^{18}O$ record (Lisiecki & Raymo, 2005); (f–h) The Earth's orbital parameters of eccentricity, obliquity and precession (Laskar et al., 2004). The black lines represent sapropels (Kidd et al., 1978), which contains more than 2% of organic carbon. The gray lines are gray layers that contains less than 2% of organic carbon. The red lines represent African monsoon index (Colleoni et al., 2012; Rossignol-Strick, 1983, 1985).

formation of which requires seasonally wet-dry variations, supports our pedogenic model for magnetic susceptibility enhancement in the VA section. Modern soils in Spain are also reported to have similar magnetic enhancement mechanisms as Chinese loess, providing further support to our interpretation (Liu et al., 2016; Torrent et al., 2006).

We note that some studies suggest that summer drying in the study area did not begin until around 3.3 Ma and before then climate was generally arid without much precipitation seasonality (Jiménez-Moreno et al., 2010; Suc, 1984; Suc & Popescu, 2005). This is consistent with lower degree of magnetic enhancement over 4–3.65 Ma for the alluvial fan deposits (Unit II), in comparison with those after ~3.5 Ma (Unit IV; Figure 1).

One difference between pedogenesis in the studied section and the CLP is that for the CLP sediments, pedogenesis occurred mostly after deposition (Maher & Thompson, 1991; Zhou et al., 1990). However, pedogenesis or chemical weathering here may have occurred over the source region, during transportation, and after deposition. That is, intensified pedogenesis, as can be inferred from increased magnetic parameter values likely driven by high insolation, reflects an integrated effect of weathering over source region, during transportation, and after deposition. Therefore, the magnetic parameter variations may indicate precipitation variations in this region instead of precipitation variations at the site of deposition. There are many references studying magnetic enhancement timing in soils and the common view is that it occurs within a couple of hundreds of years, if not shorter (Hallberg et al., 1978; Maher & Hu, 2006; Maher et al., 2003; Nie et al., 2010). Nie et al. (2015) demonstrate that storage could be a concern in places that have low relief such as the middle Yellow River. Sites bounding mountains do not belong to this category, except as local scale, and work in the Qaidam Basin demonstrates that magnetic enhancements track insolation forcing well (Nie et al., 2017; Su et al., 2019). These lines of evidence suggest that significant (on the scale of tens of thousands of years) delay of transport due to storage is unlikely in the study site, which is bound by mountains. Although we feel that these references support our working hypothesis, we admit that geomorphic factors, vegetation, and thresholds can potentially complicate our interpretations of magnetic enhancement mechanisms in Europe, especially for sites that are far from mountains. We also note that the $\chi_{fd\%}$ values are above 15% for many samples of the studied section (Figure S8 in Supporting Information S1), whereas this is rarely observed for Chinese loess. This difference indicates that the studied Spain sediments have a narrower distribution of pedogenic ferrimagnetic grains (Worm, 1998; Worm & Jackson, 1999), which may be caused by climatic difference between these two regions: summer precipitation versus winter precipitation.

In contrast with the alluvial fan sediments, magnetic parameter records do not show a strong correlation in the lacustrine sediments (Figure 2) and the magnetic susceptibility values in these two intervals (Units I and III) are more than one order of magnitude lower than those of the alluvial fan deposits (Units II and IV), with the absolute values similar to sediment in which magnetic mineral dissolution has occurred (Ao et al., 2010; Wang et al., 2021). These observations indicate that magnetic minerals might have dissolved or the carbonate intervals initially had very few magnetic minerals, and thus magnetic parameters cannot be used to infer paleo-precipitation variations in Units I and III.

### 5.2. Contrasting Orbital Cycles Between the Early and Late Pliocene Spain Records

The early Pliocene alluvial fan $\chi_{fd}$ record from the VA section provides clear evidence for insolation, instead of high latitude ice volume, forcing of the precipitation variation. Interestingly, the late Pliocene portion (ca. 3.3–3.18 Ma) shows contrasting orbital cycles in comparison with the lower portion (4–3.65 Ma).

Over the interval ca. 4–3.65 Ma, three high $\chi_{fd}$ value intervals are aligned with three high eccentricity periods (Figures 3a, 3f, 3g and 3h). Wavelet and power spectral analysis show strong 100-kyr variations, clear 20-kyr-band variations, but weak 41-kyr variations (Figure 3 and Figure S7a in Supporting Information S1). This result is consistent with regional wet-dry variations in the Mediterranean region associated with African monsoon intensity variations (Figures 3b and 3c), which reveal clear eccentricity and precession forcing.

By contrast, the 41-kyr signal is intensified over the 3.3–3.18 Ma, as can be told by three cycles over the 120-kyr interval, and the precessional signal is weak (Figure 3 and Figure S7b in Supporting Information S1). We note that this interval is characterized by low eccentricity and past research suggests that obliquity cycles can intensify in paleoclimate record during low eccentricity intervals (Holbourn et al., 2013). Abels et al. (2009) demonstrated obliquity control of lithofacies and depositional environmental variations over the interval of 405 kyr eccentricity minima, using the Miocene distal alluvial sediments within the Teruel Basin as examples. The strong obliquity cycles over 3.3–3.18 Ma corresponding to low eccentricity is consistent with the pattern reported by Abels et al. (2009). Another two intervals of 405 eccentricity minima occurred over 4.1–4 and 3.7–3.6 Ma (Figure 3). However, magnetic mineral dissolution may have destroyed the otherwise strong obliquity cycles over these two periods in the VA section. Interestingly, both 4.1–4 and 3.7–3.6 Ma correspond to lacustrine sediments, and 3.3–3.18 Ma correspond to intensified precipitation, all corresponding to wet environments, maybe a result of eccentricity forcing of environmental variations in this basin. We therefore attribute intensification of the 41-kyr cycles and weakened precession cycles over this time period to damped insolation at 20-kyr band associated with low eccentricity. Eccentricity is higher before and after than it is during 3.3–3.18 Ma and although the upper

alluvial fan $\chi_{fd}$ record from outside the eccentricity minimum is short, it contains no clear 41-kyr cycles. We interpret this as a piece of evidence suggesting insolation forcing of wet-dry variations of northeastern Spain.

The weakened precessional band signal is also observed in other regional climate records. For example, calculated African monsoon index (MI) values based on summer insolation gradient between tropics and equator (Rossignol-Strick, 1983, 1985; Colleoni et al., 2012) and observed sapropel appearances in the Mediterranean Sea sediments show weak precessional band variations over the interval ca. 3.3–3.18 Ma (Figures 3b and 3c), consistent with our findings. Even the monsoonal record from the CLP shows lower amplitude variation at the 20-kyr band in part of this interval (3.3–3.18 Ma) in comparison with the following period 3.18–3 Ma (Figure 3d). These results consistently demonstrate variability in the insolation forcing of Northern Hemisphere (NH) precipitation during the late Pliocene.

We note that it is also possible that ice sheets played a direct role in amplifying the observed clear 41-kyr wet-dry cycles in Spain and we note that the M2 event is clearly observed in the $\chi_{fd}$ record. However, the benthic oxygen isotope record shows that ice sheets had a monotonic trend from 3.3 to 3.18 Ma, inconsistent with the trend of the $\chi_{fd}$ variations in Spain (Figure 3e and Figure S9 in Supporting Information S1). Instead, the trend is more consistent with insolation variation, with the highest value at ca. 3.25 Ma and lower values at ca. 3.28 and 3.21 Ma (Figure S9 in Supporting Information S1). Therefore, ice sheets variations may have only played a minor role in accounting for the clear 41-kyr wet-dry cycles in Spain over the late Pliocene. This is in direct contrast with many Quaternary records which show dominant high latitude ice sheets forcing of regional climate (Colleoni et al., 2012; Dinarès-Turell et al., 2003; Herbert et al., 2015; Popescu et al., 2010). That said, the data do show that ice sheets could have impacted Iberian climate during certain events, such as M2 (3.3 Ma). Insolation did not show abrupt change near this time, so the climate drying slightly before 3.3 Ma, as indicated by magnetic parameter value decrease, can be reasonably interpreted by expanding NH ice sheets size (Kleiven et al., 2002), considering age model uncertainties. It is well known that ice sheets expansion and high latitude cooling could modify North Atlantic atmosphere pressure gradients and thereby change precipitation patterns in the study area.

## 6. Conclusions

We reported detailed rock magnetic analysis results on the late Pliocene alluvial-lacustrine sediments of the VA section in the Teruel Basin. Our results suggest that the magnetic enhancement in the alluvial sediments of the VA section in the Teruel Basin was likely caused by neoformation of nanometer-scale ferrimagnetic magnetite/maghemite particles during pedogenesis, similar to the situation of CLP, where more frequent oxidation/reduction cycles in soil pore space associated with seasonably wetter climate tend to produce more finer ferrimagnetic particles and higher degree of magnetic enhancement. This finding allows a deeper understanding of the precipitation variations recorded by this set of sediments. Spectral analysis results suggest that diverse manifestations of insolation forcing of climate changes in the northeastern Spain between the early and late Pliocene. For the interval 4–3.65 Ma, the wet-dry variations in Spain are dominated by eccentricity and precession cycles. By contrast, over the low eccentricity interval 3.3–3.18 Ma, obliquity forcing intensified. These results demonstrate insolation forcing of NH wet-dry variations over the Pliocene. Therefore, the periodicities of NH wet-dry variations can be largely explained by insolation variations. Without the complication of ice sheets forcing over the late Pliocene, insolation seems to be the only reasonable major forcing for NH environmental variations at the orbital bands. The importance of ice sheets for controlling Iberian climate is apparent for events such as the M2 glaciation, suggesting the growing importance of high latitude forcing with global cooling. Using the late Pliocene as an analogue, our result suggests that future climate would be primarily characterized by 20-kyr variations under natural forcing.

## Conflict of Interest

The authors declare no conflict of interest relevant to this study.

## Data Availability Statement

The data used in this paper can be obtained from the figshare website (available from https://doi.org/10.6084/m9.figshare.16959391.v2).

**Acknowledgments**
Constructive comments by three reviewers significantly improved the manuscript. The authors thank Zunbo Xu, Xingwan Liu, Zhongbao Zhang, Weihan Wang, Xiaoxue Wang, Yifan Hua, Fangbin Liu and Hansheng Wang for assistance in the experiments. This work was financially supported by the National Natural Science Foundation of China (grant 42030505, 42161144012), Second Tibetan Plateau Scientific Expedition (grant 2019QZKK0704), Science and Technology Department of Gansu Province of China (grant 20JR5RA260), the 111 Project (grant BP0618001), and National Science Foundation of the United States of America (PIRE grant 1545859).

## References

Abels, H. A., Aziz, H. A., Ventra, D., & Hilgen, F. J. (2009). Orbital climate forcing in mudflat to marginal lacustrine deposits in the Miocene Teruel Basin (Northeast Spain). *Journal of Sedimentary Research*, *79*(11), 831–847. https://doi.org/10.2110/jsr.2009.081

Ahmed, I. A. M., & Maher, B. A. (2018). Identification and paleoclimatic significance of magnetite nanoparticles in soils. *Proceedings of the National Academy of Sciences of the United States of America*, *115*(8), 1736–1741. https://doi.org/10.1073/pnas.1719186115

Alonso-Zarza, A. M., & Arenas, C. (2004). Cenozoic calcretes from the Teruel Graben, Spain: Microstructure, stable isotope geochemistry and environmental significance. *Sedimentary Geology*, *167*(1–2), 91–108. https://doi.org/10.1016/j.sedgeo.2004.02.001

Alonso-Zarza, A. M., & Calvo, J. P. (2000). Palustrine sedimentation in an episodically subsiding basin: The Miocene of the northern Teruel Graben (Spain). *Palaeogeography, Palaeoclimatology, Palaeoecology*, *160*(1–2), 1–21. https://doi.org/10.1016/S0031-0182(00)00041-9

Alonso-Zarza, A. M., Melendez, A., Martin-Garcia, R., Herrero, M. J., & Martin-Perez, A. (2012). Discriminating between tectonism and climate signatures in palustrine deposits: Lessons from the Miocene of the Teruel Graben, NE Spain. *Earth-Science Reviews*, *113*(3–4), 141–160. https://doi.org/10.1016/j.earscirev.2012.03.011

An, Z. S., Kutzbach, J. E., Prell, W. L., & Porter, S. C. (2001). Evolution of Asian monsoons and phased uplift of the Himalayan Tibetan plateau since late Miocene times. *Nature*, *411*(6833), 62–66. https://doi.org/10.1038/35075035

Anadón, P., Cabrera, L., Julia, R., Roca, E., & Rosell, L. (1989). Lacustrine oil-shale basins in tertiary Grabens from Ne Spain (Western European rift system). *Palaeogeography, Palaeoclimatology, Palaeoecology*, *70*(1–3), 7–28. https://doi.org/10.1016/0031-0182(89)90077-1

Ao, H., Deng, C., Dekkers, M. J., & Liu, Q. (2010). Magnetic mineral dissolution in pleistocene fluvio-lacustrine sediments, Nihewan basin (North China). *Earth and Planetary Science Letters*, *292*(1), 191–200. https://doi.org/10.1016/j.epsl.2010.01.035

Barrón, V., Torrent, J., & de Grave, E. (2003). Hydromaghemite, an intermediate in the hydrothermal transformation of 2-line ferrihydrite into hematite. *American Mineralogist*, *88*(11–12), 1679–1688. https://doi.org/10.2138/am-2003-11-1207

Bloemendal, J., King, J. W., Hall, F. R., & Doh, S. J. (1992). Rock magnetism of late Neogene and pleistocene deep-sea sediments – Relationship to sediment source, diagenetic processes, and sediment lithology. *Journal of Geophysical Research*, *97*(B4), 4361–4375. https://doi.org/10.1029/91jb03068

Bloemendal, J., & Liu, X. (2005). Rock magnetism and geochemistry of two plio–pleistocene Chinese loess-palaeosol sequences implications for quantitative palaeoprecipitation reconstruction. *Palaeogeography, Palaeoclimatology, Palaeoecology*, *226*(1), 149–166. https://doi.org/10.1016/j.palaeo.2005.05.008

Colleoni, F., Masina, S., Negri, A., & Marzocchi, A. (2012). Plio–pleistocene high–low latitude climate interplay: A mediterranean point of view. *Earth and Planetary Science Letters*, *319–320*, 35–44. https://doi.org/10.1016/j.epsl.2011.12.020

Dinarès-Turell, J., Hoogakker, B. A. A., Roberts, A. P., Rohling, E. J., & Sagnotti, L. (2003). Quaternary climatic control of biogenic magnetite production and eolian dust input in cores from the mediterranean sea. *Palaeogeography, Palaeoclimatology, Palaeoecology*, *190*, 195–209. https://doi.org/10.1016/s0031-0182(02)00605-3

Domingo, L., Grimes, S. T., Domingo, M. S., & Alberdi, M. T. (2009). Paleoenvironmental conditions in the Spanish miocene-pliocene boundary: Isotopic analyses of hipparion dental enamel. *Naturwissenschaften*, *96*(4), 503–511. https://doi.org/10.1007/s00114-008-0500-y

Dowsett, H., Dolan, A., Rowley, D., Moucha, R., Forte, A. M., Mitrovica, J. X., et al. (2016). The PRISM4 (mid-Piacenzian) paleoenvironmental reconstruction. *Climate of the Past*, *12*(7), 1519–1538. https://doi.org/10.5194/cp-12-1519-2016

Dowsett, H., Robinson, M., Haywood, A., Salzmann, U., Hill, D., Sohl, L., et al. (2010). The PRISM3D paleoenvironmental reconstruction. *Stratigraphy*, *7*(2–3), 123–139.

Dowsett, H., Thompson, R., Barron, J., Cronin, T., Fleming, F., Ishman, S., et al. (1994). Joint investigations of the middle Pliocene climate I: PRISM paleoenvironmental reconstructions. *Global and Planetary Change*, *9*(3), 169–195. https://doi.org/10.1016/0921-8181(94)90015-9

Emeis, K. C., Sakamoto, T., Wehausen, R., & Brumsack, H. J. (2000). The sapropel record of the eastern mediterranean sea – Results of ocean drilling program leg 160. *Palaeogeography, Palaeoclimatology, Palaeoecology*, *158*(3–4), 371–395. https://doi.org/10.1016/S0031-0182(00)00059-6

Ezquerro, L., Luzon, A., Navarro, M., Liesa, C. L., & Simon, J. L. (2014). Climatic vs. tectonic signals in a continental extensional basin (Teruel, NE Spain) from stable isotope (delta O-18) and sequence stratigraphical evolution. *Terra Nova*, *26*(5), 337–346. https://doi.org/10.1111/ter.12101

Ezquerro, L., Luzon, A., Simon, J. L., & Liesa, C. L. (2019). Alluvial sedimentation and tectono-stratigraphic evolution in a narrow extensional zigzag basin margin (northern Teruel Basin, Spain). *Journal of Palaeogeography-English*, *8*. https://doi.org/10.1186/s42501-019-0044-4

Guo, Z. T., Ruddiman, W. F., Hao, Q. Z., Wu, H. B., Qiao, Y. S., Zhu, R. X., et al. (2002). Onset of Asian desertification by 22 Myr ago inferred from loess deposits in China. *Nature*, *416*(6877), 159–163. https://doi.org/10.1038/416159a

Hallberg, G. R., Fenton, T. E., & Miller, G. A. (1978). Standard weathering zone terminology for the description of quaternary sediments in Iowa. In G. R. Hallberg (Ed.), *Standard procedures for the evaluation of quaternary materials in Iowa* (pp. 75–109). Iowa City: Iowa Geological Survey. Technical Information Series.

Haywood, A. M., Dowsett, H. J., & Dolan, A. M. (2016). Integrating geological archives and climate models for the mid-Pliocene warm period. *Nature Communications*, *7*, 10646. https://doi.org/10.1038/ncomms10646

Haywood, A. M., Dowsett, H. J., Otto-Bliesner, B., Chandler, M. A., Dolan, A. M., Hill, D. J., et al. (2010). Pliocene model intercomparison project (PlioMIP): Experimental design and boundary conditions (experiment 1). *Geoscientific Model Development*, *3*(1), 227–242. https://doi.org/10.5194/gmd-3-227-2010

Herbert, T. D., Ng, G., & Peterson, L. C. (2015). Evolution of mediterranean sea surface temperatures 3.5–1.5 Ma: Regional and hemispheric influences. *Earth and Planetary Science Letters*, *409*, 307–318. https://doi.org/10.1016/j.epsl.2014.10.006

Holbourn, A., Kuhnt, W., Clemens, S., Prell, W., & Andersen, N. (2013). Middle to late Miocene stepwise climate cooling: Evidence from a high-resolution deep water isotope curve spanning 8 million years. *Paleoceanography*, *28*(4), 688–699. https://doi.org/10.1002/2013pa002538

Hu, P. X., Liu, Q. S., Torrent, J., Barron, V., & Jin, C. S. (2013). Characterizing and quantifying iron oxides in Chinese loess/paleosols: Implications for pedogenesis. *Earth and Planetary Science Letters*, *369*, 271–283. https://doi.org/10.1016/j.epsl.2013.03.033

Jiménez-Moreno, G., Burjachs, F., Expósita, I., Oms, O., Carrancho, A., Villalaín, J. J., et al. (2013). Late Pliocene vegetation and orbital-scale climate changes from the western Mediterranean area. *Global and Planetary Change*, *108*, 15–28. https://doi.org/10.1016/j.gloplacha.2013.05.012

Jiménez-Moreno, G., Fauquette, S., & Suc, J. P. (2010). Miocene to Pliocene vegetation reconstruction and climate estimates in the Iberian Peninsula from pollen data. *Review of Palaeobotany and Palynology*, *162*(3), 403–415. https://doi.org/10.1016/j.revpalbo.2009.08.001

Jiménez-Moreno, G., Perez-Asensio, J. N., Larrasoana, J. C., Sierro, F. J., Garcia-Castellanos, D., Salazar, A., et al. (2019). Early Pliocene climatic optimum, cooling and early glaciation deduced by terrestrial and marine environmental changes in SW Spain. *Global and Planetary Change*, *180*, 89–99. https://doi.org/10.1016/j.gloplacha.2019.06.002

Kidd, R. B., Cita, M. B., & Ryan, W. (1978). Stratigraphy of eastern Mediterranean sapropel sequences recovered during DSDP Leg 42A and their paleoenvironmental significance. In *Proceedings of the Ocean Drilling Program Initial Reports 42A* (Vol. 42, pp. 421–443). Washington: U.S. Goverment Printing Office. https://doi.org/10.2973/dsdp.proc.42-1.113-1

Kleiven, H. F., Jansen, E., Fronval, T., & Smith, T. M. (2002). Intensification of Northern hemisphere glaciations in the circum Atlantic region (3.5–2.4 Ma) – Ice-rafted detritus evidence. *Palaeogeography, Palaeoclimatology, Palaeoecology*, *184*(3–4), 213–223. https://doi.org/10.1016/S0031-0182(01)00407-2

Laskar, J., Robutel, P., Joutel, F., Gastineau, M., Correia, A. C. M., & Levrard, B. (2004). A long-term numerical solution for the insolation quantities of the Earth. *Astronomy and Astrophysics*, *428*(1), 261–285. https://doi.org/10.1051/0004-6361:20041335

Li, M., Hinnov, L., & Kump, L. (2019). Acycle: Time-series analysis software for paleoclimate research and education. *Computers & Geosciences*, *127*, 12–22. https://doi.org/10.1016/j.cageo.2019.02.011

Li, Y. R., Shi, W. H., Aydin, A., Beroya-Eitner, M. A., & Gao, G. H. (2020). Loess genesis and worldwide distribution. *Earth-Science Reviews*, *201*. https://doi.org/10.1016/j.earscirev.2019.102947

Lisiecki, L. E., & Raymo, M. E. (2005). A Pliocene-Pleistocene stack of 57 globally distributed benthic $\delta^{18}O$ records. *Paleoceanography*, *20*(2). https://doi.org/10.1029/2004PA001071

Liu, Q. S., Jackson, M. J., Banerjee, S. K., Maher, B. A., Deng, C. L., Pan, Y. X., et al. (2004). Mechanism of the magnetic susceptibility enhancements of the Chinese loess. *Journal of Geophysical Research*, *109*(B12). https://doi.org/10.1029/2004JB003249

Liu, Q. S., Zhang, C. X., Torrent, J., Barron, V., Hu, P. X., Jiang, Z. X., et al. (2016). Factors controlling magnetism of reddish Brown soil profiles from calcarenites in southern Spain: Dust inputor in-situ pedogenesis? *Frontiers of Earth Science*, *4*(51). https://doi.org/10.3389/feart.2016.00051

Liu, Z. F., Liu, Q. S., Torrent, J., Barron, V., & Hu, P. X. (2013). Testing the magnetic proxy chi(FD)/HIRM for quantifying paleoprecipitation in modern soil profiles from Shaanxi Province, China. *Global and Planetary Change*, *110*, 368–378. https://doi.org/10.1016/j.gloplacha.2013.04.013

Luo, Z., Nie, J., Moe, A. E., Heermance, R. V., Garzione, C., Herbert, T. D., et al. (2020). Joint insolation and ice sheet/$CO_2$ forcing on northern China precipitation during Pliocene warmth. *Science Bulletin*, *66*(4), 319–322. https://doi.org/10.1016/j.scib.2020.10.025

Maher, B. A. (1998). Magnetic properties of modern soils and quaternary loessic paleosols: Paleoclimatic implications. *Palaeogeography, Palaeoclimatology, Palaeoecology*, *137*(1), 25–54. https://doi.org/10.1016/S0031-0182(97)00103-X

Maher, B. A., Alekseev, A., & Alekseeva, T. (2003). Magnetic mineralogy of soils across the Russian steppe: Climatic dependence of pedogenic magnetite formation. *Palaeogeography, Palaeoclimatology, Palaeoecology*, *201*(3–4), 321–341. https://doi.org/10.1016/S0031-0182(03)00618-7

Maher, B. A., & Hu, M. (2006). A high-resolution record of holocene rainfall variations from the western Chinese loess Plateau: Antiphase behaviour of the African/Indian and east Asian summer monsoons. *The Holocene*, *16*(3), 309–319. https://doi.org/10.1191/0959683606hl929rp

Maher, B. A., & Taylor, R. M. (1988). Formation of ultrafine-grained magnetite in soils. *Nature*, *336*(6197), 368–370. https://doi.org/10.1038/336368a0

Maher, B. A., & Thompson, R. (1991). Mineral magnetic record of the Chinese loess and paleosol. *Geology*, *19*(1), 32–36. https://doi.org/10.1130/0091-7613(1991)019<0003:MMROTC>2.3.CO

Nie, J., King, J. W., & Fang, X. (2007). Enhancement mechanisms of magnetic susceptibility in the Chinese red-clay sequence. *Geophysical Research Letters*, *34*(19). https://doi.org/10.1029/2007gl031430

Nie, J., Song, Y., King, J. W., & Egli, R. (2010). Consistent grain size distribution of pedogenic maghemite of surface soils and Miocene loessic soils on the chinese loess plateau. *Journal of Quaternary Science*, *25*(3), 261–266. https://doi.org/10.1002/jqs.1304

Nie, J., Stevens, T., Rittner, M., Stockli, D., Garzanti, E., Limonta, M., et al. (2015). Loess plateau storage of Northeastern tibetan plateau-derived yellow river sediment. *Nature Communications*, *6*, 8511. https://doi.org/10.1038/ncomms9511

Nie, J. S., Garzione, C., Su, Q. D., Liu, Q. S., Zhang, R., Heslop, D., et al. (2017). Dominant 100,000-year precipitation cyclicity in a late Miocene lake from northeast Tibet. *Science Advances*, *3*(3). https://doi.org/10.1126/sciadv.1600762

Nie, J. S., Ren, X. P., Saylor, J. E., Su, Q. D., Horton, B. K., Bush, M. A., et al. (2020). Magnetic polarity stratigraphy, provenance, and paleoclimate analysis of Cenozoic strata in the Qaidam Basin, NE Tibetan Plateau. *The Geological Society of America Bulletin*, *132*(1–2), 310–320. https://doi.org/10.1130/B35175.1

Ogg, J. G. (2020). Chapter 5 – Geomagnetic polarity time scale. In F. M. Gradstein, J. G. Ogg, M. D. Schmitz, & G. M. Ogg (Eds.), *Geologic time scale 2020* (pp. 159–192). Elsevier. https://doi.org/10.1016/B978-0-12-824360-2.00005-X

Opdyke, N., Mein, P., Lindsay, E., PerezGonzales, A., Moissenet, E., & Norton, V. L. (1997). Continental deposits, magnetostratigraphy and vertebrate paleontology, late Neogene of Eastern Spain. *Palaeogeography, Palaeoclimatology, Palaeoecology*, *133*(3–4), 129–148. https://doi.org/10.1016/S0031-0182(97)00080-1

Palchan, D., Neugebauer, I., Amitai, Y., Waldmann, N. D., Schwab, M. J., Dulski, P., et al. (2017). North Atlantic controlled depositional cycles in MIS 5e layered sediments from the deep Dead Sea basin. *Quaternary Research*, *87*, 168. https://doi.org/10.1017/qua.2016.10

Popescu, S. M., Biltekin, D., Winter, H., Suc, J.P., Melinte-Dobrinescu, M. C., Klotz, S., et al. (2010). Pliocene and Lower Pleistocene vegetation and climate changes at the European scale: Long pollen records and climatostratigraphy. *Quaternary International*, *219*(1–2), 152–167. https://doi.org/10.1016/j.quaint.2010.03.013

Roca, E., & Guimerà, J. (1992). The Neogene structure of the eastern iberian margin – Structural constraints on the crustal evolution of the valencia trough (Western mediterranean). *Tectonophysics*, *203*(1–4), 203–218. https://doi.org/10.1016/0040-1951(92)90224-T

Rossignol-Strick, M. (1983). African monsoons, an immediate climate response to orbital insolation. *Nature*, *304*(5921), 46–49. https://doi.org/10.1038/304046a0

Rossignol-Strick, M. (1985). Mediterranean quaternary sapropels, an immediate response of the African monsoon to variation of insolation. *Palaeogeography, Palaeoclimatology, Palaeoecology*, *49*(3), 237–263. https://doi.org/10.1016/0031-0182(85)90056-2

Salzmann, U., Williams, M., Haywood, A. M., Johnson, A. L. A., Kender, S., & Zalasiewicz, J. (2011). Climate and environment of a Pliocene warm world. *Palaeogeography, Palaeoclimatology, Palaeoecology*, *309*(1), 1–8. https://doi.org/10.1016/j.palaeo.2011.05.044

Su, Q., Nie, J., Meng, Q., Heermance, R., Gong, L., Luo, Z., et al. (2019). Central Asian drying at 3.3 Ma linked to tropical forcing? *Geophysical Research Letters*, *46*(17–18), 10561–10567. https://doi.org/10.1029/2019GL084648

Suc, J. P. (1984). Origin and evolution of the mediterranean vegetation and climate in Europe. *Nature*, *307*(5950), 429–432. https://doi.org/10.1038/307429a0

Suc, J. P., & Popescu, S. M. (2005). Pollen records and climatic cycles in the North Mediterranean region since 2.7 Ma. *Early-Middle Pleistocene Transitions: The Land-Ocean Evidence*, *247*, 147–158. https://doi.org/10.1144/Gsl.Sp.2005.247.01.08

Sun, Y. B., Clemens, S. C., An, Z. S., & Yu, Z. W. (2006). Astronomical timescale and palaeoclimatic implication of stacked 3.6-Myr monsoon records from the chinese loess plateau. *Quaternary Science Reviews*, *25*(1–2), 33–48. https://doi.org/10.1016/j.quascirev.2005.07.005

Tauxe, L. (1998). *Paleomagnetic principles and practice, modern approaches in geophysics* (pp. 300). Springer. https://doi.org/10.1007/0-306-48128-6

Torrent, J., Barrón, V., & Liu, Q. S. (2006). Magnetic enhancement is linked to and precedes hematite formation in aerobic soil. *Geophysical Research Letters*, *33*, L02401. https://doi.org/10.1029/2005gl024818

Van Dam, J. A., Alcala, L., Alonso-Zarza, A. M., Calvo, J. P., Garces, M., & Krijgsman, W. (2001). The upper Miocene mammal record from the Teruel-Alfambra region (Spain). The MN system and continental stage/age concepts discussed. *Journal of Vertebrate Paleontology*, *21*, 367–385. https://doi.org/10.1671/0272-4634(2001)021[0367:Tummrf]2.0.Co;2

Waldmann, N., Stein, M., Ariztegui, D., & Starinsky, A. (2009). Stratigraphy, depositional environments and level reconstruction of the last interglacial Lake Samra in the Dead Sea basin. *Quaternary Research*, *72*(1), 1–15. https://doi.org/10.1016/j.yqres.2009.03.005

Wang, X. X., Nie, J. S., & Saylor, J. E. (2021). Anti-phase strengthening of the south and east asian summer monsoons during the early Pliocene driven by southern hemisphere ice volume. *Paleoceanography and Paleoclimatology*, *36*(5). https://doi.org/10.1029/2021PA004211

Worm, H. (1998). On the superparamagnetic-stable single domain transition for magnetite, and frequency dependence of susceptibility. *Geophysical Journal International*, *133*(1), 201–206. https://doi.org/10.1046/j.1365-246X.1998.1331468.x

Worm, H., & Jackson, M. (1999). The superparamagnetism of Yucca mountain tuff. *Journal of Geophysical Research*, *104*(B11), 25415–25425. https://doi.org/10.1029/1999JB900285

Zhou, L. P., Oldfield, F., Wintle, A. G., Robinson, S. G., & Wang, J. T. (1990). Partly pedogenic origin of magnetic variations in chinese loess. *Nature*, *346*, 737–739. https://doi.org/10.1038/346737a0

## References From the Supporting Information

Anson, G. L., & Kodama, K. P. (1987). Compaction-induced inclination shallowing of the post-depositional remanent magnetization in a synthetic sediment. *Geophysical Journal of the Royal Astronomical Society*, *88*, 673–692. https://doi.org/10.1111/j.1365-246X.1987.tb01651.x

Fisher, R. (1953). Dispersion on a sphere. *Proceedings of the Royal Society A: Mathematical, Physical & Engineering Sciences*, *217*(1130), 295–305. https://doi.org/10.1098/rspa.1953.0064

Jones, C. H. (2002). User-driven integrated software lives: "Paleomag" paleomagnetics analysis on the macintosh. *Computers and Geosciences*, *28*(10), 1145–1151. https://doi.org/10.1016/s0098-3004(02)00032-8

Kirschvink, J. L. (1980). The least-squares line and plane and the analysis of palaeomagnetic data. *Geophysical Journal International*, *62*(3), 699–718. https://doi.org/10.1111/j.1365-246X.1980.tb02601.x

Kodama, K. P. (1997). A successful rock magnetic technique for correctng paleomagnetic inclination shallowing: Case study of the Nacimiento Formation, New Mexico. *Journal of Geophysical Research: Solid Earth*, *102*(B3), 5193–5205. Retrieved from https://go.exlibris.link/6M7yChXZ

Lourens, L. J. (2004). Revised tuning of ocean drilling program site 964 and KC01B (Mediterranean) and implications for the $\delta^{18}O$, tephra, calcareous nannofossil, and geomagnetic reversal chronologies of the past 1.1 Myr. *Paleoceanography*, *19*(3). https://doi.org/10.1029/2003pa000997

Lourens, L. J., Antonarakou, A., Hilgen, F. J., VanHoof, A. A. M., VergnaudGrazzini, C., & Zachariasse, W. J. (1996). Evaluation of the Plio-Pleistocene astronomical timescale. *Paleoceanography*, *11*(4), 391–413. https://doi.org/10.1029/96pa01125

Mann, M. E., & Lees, J. M. (1996). Robust estimation of background noise and signal detection in climatic time series. *Climatic Change*, *33*(3), 409–445. https://doi.org/10.1007/Bf00142586

Nie, J., Song, Y., & King, J. W. (2016). A review of recent advances in red-clay environmental magnetism and paleoclimate history on the chinese loess plateau. *Frontiers of Earth Science*, *4*. https://doi.org/10.3389/feart.2016.00027

Pike, C. R., Roberts, A. P., & Verosub, K. L. (2001). First-order reversal curve diagrams and thermal relaxation effects in magnetic particles. *Geophysical Journal International*, *145*(3), 721–730. https://doi.org/10.1046/j.0956-540x.2001.01419.x

Roberts, A. P., Pike, C. R., & Verosub, K. L. (2000). First-order reversal curve diagrams: A new tool for characterizing the magnetic properties of natural samples. *Journal of Geophysical Research*, *105*(B12), 28461–28475. https://doi.org/10.1029/2000JB900326

Tan, X., & Kodama, K. P. (2002). Magnetic anisotropy and paleomagnetic inclination shallowing in red beds: Evidence from the Mississippian Mauch Chunk formation, Pennsylvania. *Journal of Geophysical Research*, *107*(B11)–2311. https://doi.org/10.1029/2001JB001636

Torrence, C., & Compo, G. P. (1998). A practical guide to wavelet analysis. *Bulletin of the American Meteorological Society*, *79*(1), 61–78. https://doi.org/10.1175/1520-0477(1998)079<0061:Apgtwa>2.0.Co

Zijderveld, J. D. A. (1967). Demagnetization of rocks: Analysis of results. *Developments in Solid Earth Geophysics*, *3*, 245–286. https://doi.org/10.1016/B978-1-4832-2894-5.50049-5